EUROPEAN ORGANIZATION FOR NUCLEAR RESEARCH

CERN-EP/86-160
3 November 1986

STRANGENESS PRODUCTION IN DEEP INELASTIC MUON NUCLEON SCATTERING AT 280 GeV

The European Muon Collaboration

Aachen[1], CERN[2], DESY (Hamburg)[3], Freiburg[4], Hamburg (University)[5], Kiel[6], LAL (Orsay)[7], Lancaster[8], LAPP (Annecy)[9], Liverpool[10], Marseille[11], Mons[12], MPI (München)[13], Oxford[14], RAL (Chilton)[15], Sheffield[16], Torino[17], Uppsala[18], Warsaw[19], Wuppertal[20].

M. Arneodo[17], A. Arvidson[18], J.J. Aubert[11], B. Badelek[19a)], J. Beaufays[2], C.P. Bee[8b)], C. Benchouk[11], G. Berghoff[1], I. Bird[8c)], D. Blum[7], E. Böhm[6], X. de Bouard[9], F.W. Brasse[3], H. Braun[20], C. Broll[9+)], S. Brown[10d)], H. Brück[20e)], H. Calen[18], J.S. Chima[15f)], J. Ciborowski[19a], R. Clifft[15], G. Coignet[9], F. Combley[16], J. Coughlan[8g)], G. D'Agostini[11], S. Dahlgren[18], F. Dengler[13], I. Derado[13], T. Dreyer[4], J. Drees[20], M. Düren[1], V. Eckardt[13], A. Edwards[20h)], M. Edwards[15], T. Ernst[4], G. Eszes[9i)], J. Favier[9], M.I. Ferrero[17], J. Figiel[5j)], W. Flauger[3], J. Foster[16k)], E. Gabathuler[10], J. Gajewski[5], R. Gamet[10], J. Gayler[3], N. Geddes[14g)], P. Grafström[18], F. Grard[12], J. Haas[4], E. Hagberg[18], F.J. Hasert[11l)], P. Hayman[10], P. Heusse[7], M. Jaffré[7], A. Jacholkowska[2], F. Janata[5], G. Jancso[13i)], A.S. Johnson[14m)], E.M. Kabuss[4], G. Kellner[2], V. Korbel[3], J. Krüger[20e)], S. Kullander[18], U. Landgraf[4], D. Lanske[1], J. Loken[14], K. Long[14n)], M. Maire[9], P. Malecki[13], A. Manz[13], S. Maselli[13], W. Mohr[4], F. Montanet[11], H.E. Montgomery[20)], E. Nagy[9i)], J. Nassalski[19p)], P.R. Norton[15], F.G. Oakham[15q)], A.M. Osborne[2], C. Pascaud[7], B. Pawlik[13], P. Payre[11], C. Peroni[17], H. Peschel[20], H. Pessard[9], J. Pettingale[10], B. Pietrzyk[11], B. Pönsgen[5], M. Pötsch[20], P. Renton[14], P. Ribarics[9i)], K. Rith[4c)], E. Rondio[19a)], A. Sandacz[19p)], M. Scheer[1], A. Schlagböhmer[4], H. Schiemann[5], N. Schmitz[13], M. Schneegans[9], M. Scholz[1], T. Schröder[4], M. Schouten[13], K. Schultze[1], T. Sloan[8], H.E. Stier[4], M. Studt[5], G.N. Taylor[14], J.M. Thénard[9], J.C. Thompson[15], A. de la Torre[5r)], J. Toth[9i)], L. Urban[1], L. Urban[9i)], W. Wallucks[4], M. Whalley[16s)], S. Wheeler[16], W.S.C. Williams[14], S.J. Wimpenny[10n)], R. Windmolders[12], .

(Submitted to Zeits. für Physik C)

Abstract

The production of strange particles has been studied in a 280 GeV muon nucleon scattering experiment with acceptance and particle identification over a large kinematical range. The data show that at large values of x_{Bj} the interactions take place mostly on a u valence quark in agreement with the basic quark-parton model predictions. This feature results in a strong forward-backward asymmetry in the distribution of strangeness along the rapidity axis. The data are compatible with a strange to non-strange quark suppression factor of ≈ 0.3 and with a strong suppression of strange diquarks. The distributions of K^+K^- pairs show that the two kaons are preferentially produced at neighbouring values of rapidity.

For footnotes see next page

Addresses

1) III. Physikalisches Inst. A, Physikzentrum, Aachen, Germany.
2) CERN, Geneva, Switzerland.
3) DESY, Hamburg, Germany.
4) Fakultät für Physik, Universität Freiburg, Germany.
5) II. Institut für Experimentalphysik, Universität Hamburg, Germany.
6) II. Institut für Kernphysik, Universität Kiel, Germany.
7) Laboratoire de l'Accélérateur Linéaire, Université de Paris-Sud, Orsay, France.
8) Department of Physics, University of Lancaster, England.
9) Laboratoire d'Annecy de Physique des Particules, IN2P3, Annecy-le-Vieux, France.
10) Department of Physics, University of Liverpool, England.
11) Centre de Physique des Particules, Faculté des Sciences de Luminy, Marseille, France.
12) Faculté des Sciences, Université de L'Etat à Mons, Belgium.
13) Max-Planck-Institut für Physik und Astrophysik, München, Germany.
14) Nuclear Physics Laboratory, University of Oxford, England.
15) Rutherford and Appleton Laboratory, Chilton, Didcot, England.
16) Department of Physics, University of Sheffield, England.
17) Istituto di Fisica, Università di Torino, Italy.
18) Gustav Werners Institut, University of Uppsala, Sweden.
19) Physics Institute, University of Warsaw, and Institute for Nuclear Studies, Warsaw, Poland.
20) Fachbereich Physik, Universität Wuppertal, Germany.

a) University of Warsaw, Poland.
b) Now at University of Liverpool, England.
c) Now at MPI für Kernphysik, Heidelberg, Germany.
d) Now at TESA S.A., Renens, Switzerland.
e) Now at DESY, Hamburg, W. Germany.
f) Now at British Telecom, London, England.
g) Now at RAL, Chilton, Didcot, England.
h) Now at Jet, Joint Undertaking, Abingdon, England.
i) Permanent address: Central Research Institute for Physics of the Hungarian Academy of Science, Budapest, Hungary.
j) Now at Institute of Nuclear Physics, Krakow, Poland.
k) Now at University of Manchester, England.
l) Now at Krupp Atlas Elektronic GmbH, Bremen, Germany.
m) Now at SLAC, Stanford, California.
n) Now at CERN, Geneva, Switzerland.
o) Now at FNAL, Batavia, Illinois, U.S.A.
p) Institute for Nuclear Studies, Warsaw, Poland.
q) Now at NRC, Ottawa, Canada.
r) Now at Universidad Nacional, Mar del Plata, Argentina.
s) Now at University of Durham, England.
+) Deceased.

1. Introduction

Previous experiments have shown that hadron production in deep inelastic scattering of electrons or muons can be successfully described in the framework of the quark-parton model modified by the quantum chromodynamic effects [1]. However, the dynamics of the photon-quark interaction is obscured by the subsequent fragmentation process which at present can only be described with the help of phenomenological models [2,3], where features such as the production of diquarks, of strange quarks and of strange diquarks are represented by free parameters. The analysis of experimental results (mainly from e^+e^- annihilation) in the framework of fragmentation models has provided the basic values of these parameters [4]. Their determination in deep inelastic lepton nucleon scattering has only been partially achieved [5] due to the lack of particle identification and limited acceptance of most experiments.

In this paper, we present an analysis of strange particle production ($K^{\pm}$, K°, $\bar{\Lambda}$, Λ,) based on new data obtained in a 280 GeV muon experiment at CERN with almost full geometrical acceptance and particle identification over a wide momentum range. Due to their different quark content, strange mesons are expected to provide information on the basic quark-parton process and on the production of strangeness in the current fragmentation region. Similarly Λ production will be directly related to the target fragmentation.

After a presentation of the experimental apparatus and a discussion of the various aspects of the particle identification, we will present the inclusive spectra of strange particles and the dependence of the average multiplicities on the total centre of mass energy. In subsequent sections, we will investigate different aspects of strangeness correlations such as the compensation of strangeness along the rapidity axis, possible short range correlations of particles with opposite strangeness and the relative suppression of $\Lambda\ \bar{\Lambda}$ pairs. Results, based on partial statistics, on the production of neutral strange particles and of identified charged particles have already been published [6,7].

2. The Experimental Procedure

The data used in this analysis were obtained in a muon-nucleon scattering experiment performed at the CERN SPS (NA9 experiment). A one metre long target of liquid hydrogen or deuterium located inside a large vertex detector system was exposed to a 280 GeV positive muon beam. A forward spectrometer was used to detect and measure the scattered muon and the fast charged particles. A detailed description of the apparatus has been published previously [8] and we will only discuss here questions relevant to the present analysis, namely the identification of strange particles, the observation of neutral decays and the corresponding acceptance corrections.

In order to restrict the sample of events to kinematic regions where the corrections for event acceptance and where smearing effects from resolution and radiative corrections are relatively small, the range of deep inelastic variables was limited to:

$$Q^2 > 4 \text{ GeV}^2$$
$$16 < W^2 < 400 \text{ GeV}^2$$
$$\nu < 0.9\, E_{beam}$$
$$20 < \nu < 260 \text{ GeV}$$
$$\theta_\mu > 0.5°$$

where $-Q^2$ and ν are the four-momentum squared and the laboratory energy transferred between the incident and outgoing muons, W the total centre of mass energy of the final state hadrons and θ_μ the scattering angle of the muon in the laboratory system. The numbers of events remaining after these cuts are 28859 and 22470 for hydrogen and deuterium, respectively. In the analysis of strangeness pair production (section 5), a higher limit on W^2 has been used ($W^2<484$ GeV^2) resulting in an increase of 14% in the number of events.

As mentioned in ref. [8] high energy tracks ($P \gtrsim 6$ GeV/c) are reconstructed in the forward spectrometer while low energy tracks are

measured in the streamer chamber and extrapolated through the large angle spectrometer. Tracks from both detectors are used in the geometrical reconstruction programme to determine the primary vertex and vertices corresponding to secondary interactions in the target or to neutral particle decays. At a later stage, the position of the primary vertex is used to search for possible additional tracks of intermediate momentum among the remaining hits in the large angle spectrometer.

Monte Carlo events are generated according to the Lund model [3] including bremsstrahlung photons from the incident and scattered muons, secondary interactions in the target and a full simulation of detector responses, taking into account chamber efficiencies and measurement errors. This sample is processed in the same way as real events so as to provide a realistic estimate of apparatus acceptances and software efficiencies.

2.1 Identification of Charged Kaons

Charged particle identification is provided by an extensive set of detectors: a time of flight hodoscope system (TOF), two silica aerogel Cerenkov counters (CA) and two gas Cerenkov counters (C0 and C1) cover the low and intermediate momentum range. A large gas Cerenkov counter (C2) filled with neon is used to identify fast hadrons in the forward spectrometer.

For each track, the probability of obtaining the observed signal (pulse height or time of flight) for an assumed particle mass (e, π, K, p) is determined for each detector, taking into account measured efficiencies and background contributions [7]. The product of these conditional probabilities is then used as an estimator for the mass hypothesis. Cuts, determined by simulation studies, are applied to the estimators in order to remove those particles for which several hypotheses cannot be unambiguously separated. The contamination from non-strange charged particles (mostly pions) in the final sample of charged kaons obtained in this way is estimated by the simulation to be less than 20%.

In practice, the kaon mass can only be assigned to a measured track if the pion and the proton hypotheses are both excluded. When threshold Cerenkov counters are used, this implies that information from at least two detectors has to be combined in order to avoid the π-K and K-p ambiguities. Additional momentum cuts have been applied in order to avoid critical threshold regions in the Cerenkov counters, such as the CO-CA overlap region around 3 GeV/c. The resulting kaon identification momentum ranges (fig. 1) show that charged kaon identification is not possible for tracks with momenta between 2 and 12 GeV/c, or between 17 and 21 GeV/c, or above 38 GeV/c. These discontinuities in the charged kaon acceptance as a function of the laboratory momentum result in large losses in the central regions of cms rapidity (fig. 2) where the distributions of charged kaons cannot be reliably corrected. The central part of these distributions, shown by the shaded area in fig. 2a,b, is therefore excluded in the determination of longitudinal distributions. For average multiplicities, a global acceptance correction is provided by the ratio of generated to accepted Monte Carlo events. This implies that the correction relies strongly on the model used for the generation in the regions where the experimental acceptance is close to zero. This assumption is however, supported by the good agreement observed between corrected distributions and the model in all other kinematic regions.

2.2 Selection of Neutral Strange Particles

Since the decay vertices of the neutral strange particles are in general not directly observable in the streamer chamber, their reconstruction is based entirely on the geometric and kinematic constraints. All pairs of tracks with opposite charge and having at least one of the tracks not fitting to the primary vertex are tested in turn. When an intersection point is found, the mass of the corresponding decay particle is required to be compatible with the K^0 or the Λ mass and its direction compatible with the position of the primary vertex within 5 standard deviations.

This procedure, applied in the geometry programme, provides a basic sample of neutral strange particle candidates (V°) with a large background from secondary interactions: as expected, the initial sample of V° candidates is larger in deuterium (0.33 per event) than in hydrogen (0.25 per event). The application of more restrictive cuts on the 3-constraint fit probability removes most of the accidental associations or secondary interactions and reduces the V° sample to 0.04 per event for each target. The compatibility of the mass of each decay particle with the time of flight and Cerenkov information is also tested and the remaining kinematic ambiguities (<15%) are resolved on the basis of the best probability. The acceptances as a function of cms rapidity for K° and Λ and $\bar{\Lambda}$ are shown in fig. 2c-e. Simulation studies show that the background contamination in the final sample is of the order of 20% for K°'s and Λ's and of the order of 40% for $\bar{\Lambda}$'s. Corrections for these backgrounds are also included in the Monte Carlo simulation.

2.3 Systematic Uncertainties

Despite the use of a complete Monte Carlo simulation of the apparatus, the corrections for losses and contaminations may still suffer from systematic uncertainties. Detailed studies involving small changes of the selection criteria and internal consistency checks show that they mostly affect the overall normalisation and may be as big as 25% for both charged and neutral particles. The shape of the distributions can also be slightly distorted because of different systematic effects in different parts of the apparatus acceptance. As an example, systematic effects could be different in the three momentum ranges where charged kaons are identified by different sets of detectors. The correction to the V° sample could also be different for neutral particle cms rapidity y below 1, where most tracks are measured in the streamer chamber, and for y>1 where they are reconstructed in the forward spectrometer.

3. Inclusive Distributions

3.1 x_F Distributions

The distributions of the reduced longitudinal centre of mass momentum $x_F = p_{\parallel}/p_{max}$, corrected for acceptance and for unseen decay modes and normalised to the total number of interactions, are shown in fig. 3 for K^+, K^-, $K^\circ + \bar{K}^\circ$, $\Lambda(\Sigma^\circ)$, $\bar{\Lambda}(\bar{\Sigma}^\circ)$ particles and for the hydrogen and deuterium data sets. The K^- spectrum is found to be lower than the K^+ spectrum over the full range of x_F and equal, within the systematic errors, to the neutral kaon spectrum ($K^\circ+\bar{K}^\circ$), when scaled by a factor of 1/2. These features reproduce the basic expectations of the quark-parton model. The $\bar{\Lambda}$ and Λ rates decrease in a similar way in the forward hemisphere, but strongly differ in the backward region where Λ's are copiously produced from target remnants.

Within the limits of the statistical and the systematical errors, there is no significant difference between the hydrogen and deuterium samples, which will be combined in the rest of this analysis.

3.2 Rapidity Distributions

The cms rapidity distributions are shown in fig. 4. The curves represent the predictions of the Lund string model[1] [3] with a relative strange quark to non-strange quark suppression γ_s/γ_u of 0.3, a diquark to quark production ratio of 0.065, a relative strange diquark suppression $(\gamma_{us}/\gamma_{ud})/(\gamma_s/\gamma_u)$ of 0.2 and pseudoscalar to vector meson production ratio of 1. For charged kaons, the model predictions are slightly lower than (but consistent with) the data points while for K°'s they are systematically 15 to 20% above the data. These differences are, however, within the range of the systematic errors quoted in the previous section.

Although the gross effect of target fragmentation is clearly seen in the Λ rapidity distribution, the data points fall much lower than the predicted curve for $-2.0<y(\Lambda)<0$. On the other hand, the model is

---

1 In all figures, the Lund model predictions were obtained with version 4.3.

reasonably consistent with the data for Λ production in the forward hemisphere and for $\bar{\Lambda}$ production throughout the rapidity range. These results indicate that the fragmentation of target remnants into strange baryons is somewhat overestimated in the model.

3.3 Strangeness Compensation

As an alternative way to analyse strangeness production, we present in fig. 5a the y distributions of the average strangeness for mesons and baryons respectively, namely the differences:

$$\frac{1}{N_{ev}} \left(\frac{dN(K^+)}{dy} - \frac{dN(K^-)}{dy}\right) \text{ and } \frac{1}{N_{ev}} \left(\frac{dN(\bar{\Lambda})}{dy} - \frac{dN(\Lambda)}{dy}\right)$$

The former remains positive over the full rapidity range, while the latter shows a strong dip at negative y due to the abundant Λ production in the target fragmentation region and tends to zero in the forward region where Λ and $\bar{\Lambda}$ productions are equal.

The resulting y distribution of the total observable average strangeness (fig. 5b)

$$\frac{d\langle S\rangle}{dy} = \frac{1}{N_{ev}} \left(\frac{dN(K^+) - dN(K^-) + dN(\bar{\Lambda}) - dN(\Lambda)}{dy}\right)$$

shows an asymmetry pattern, with a somewhat larger contribution of positive strangeness in the forward hemisphere than negative strangeness in the backward hemisphere. The comparison with the Lund model predictions shows a discrepancy for $y<0$, which is a direct consequence of that observed before (fig. 4d) for Λ production in the target fragmentation region.

Since the total strangeness of the final state hadrons should be zero from strangeness conservation, our results imply that the undetected strange particles (central rapidity $K^{\pm}$, very slow Λ's and also Σ^+,

Σ^-, Ξ^- ...) and particles with unknown strangeness (i.e. neutral kaons) have predominantly negative strangeness. In the Lund model, neutral kaons are more frequently of positive than of negative strangeness.

In order to analyse the dependence of the strangeness asymmetry on the flavour of the struck quark, we present in fig. 5c the average strangeness in the forward and backward hemisphere for 3 intervals of $x_{Bj}=Q^2/2M\nu$. The mean strangeness, in the backward hemsiphere, is negative and independent of x_{Bj}. In the forward hemisphere, the average strangeness is compatible with zero for $x_{Bj}<0.05$ and increases rapidly for higher values of x_{Bj}. This suggests that the strangeness asymmetry could have the same origin as the charge retention effect [10]: the dominance of leading particles including a u quark results in an excess of mesons containing $\bar{s}$ quark over those containing an s quark in the forward direction at sufficiently large x_{Bj}. The Lund model predicts a somewhat smoother dependence of the mean forward strangeness on x_{Bj} and a negative and almost constant mean strangeness in the backward hemisphere [1].

4. Average Multiplicites of Strange Particles

The average multiplicity of the various strange particles is given in table 1 for 8 bins of the total hadronic mass W. The values presented here are for hydrogen only, in order to allow the comparison with the published averaged charged multiplicities [11]. The rise of the multiplicity with W is seen to be much slower than Λ than for $\bar{\Lambda}$, a feature expected if the Λ's are often produced as target fragments.

The ratio R_1 of the average kaon multiplicity to the total charged particle multiplicity (table 2) increases strongly between the two first W bins and continues to increase over the full W range reaching a value of ≈ 0.19 for $16<W<20$ GeV.

---

1 Another version of the Lund Monte Carlo (version 5.25, "symmetric fragmentation") yields a slightly steeper dependence of the mean forward strangeness but is still incompatible with the data.

For comparison, the values of R_1 derived from the Lund string model, with the parameters quoted in section 3, are also given in table 2. The reduction of strange particle production at the lowest W values (i.e. close to threshold) is stronger in the data than in the model. At higher W (W>6 GeV) the values of R_1 for the data and for the model are equal on average but the data show a slightly steeper increase with W (fig. 6).

A linear interpolation between the model predictions for different values of the parameter give as best estimate for the range 6<W< 20 GeV:

$$\gamma_s/\gamma_u = 0.30 \pm 0.01 \text{ (stat.)} \pm 0.07 \text{ (syst.)}.$$

Similar derivations based on charged or neutral kaons separately lead to values of 0.36 and 0.24.

Figure 7 shows the values of γ_s/γ_u for this and other measurements [9] as a function of W. The different measurements are consistent within the errors at similar values of W. The variation of γ_s/γ_u with W seems relatively small taking into account the fact that different values are obtained under very different experimental conditions. This confirms that the relative strange quark suppression is rather constant in all fragmentation processes.

5. Production of Strange Particle Pairs

The numbers of pairs of strange particles observed in the combined hydrogen and deuterium samples are listed in table 3. In the same table we also give the ratios $R_{ij} = \langle n_{ij} \rangle / (\langle n_i \rangle \langle n_j \rangle)$, where $\langle n_i \rangle (\langle n_j \rangle)$ is the average multiplicity of particle i (j) and $\langle n_{ij} \rangle$ is the average multiplicity of ij pairs. For low multiplicities, R_{ij} is approximately equal to the ratio of the average multiplicity $\langle n_j \rangle_i$ of particles j in the events also containing a particle of type i ("trigger" particle), to the overall average multiplicity $\langle n_j \rangle$ of particle j. The acceptance correction to these ratios (<20%) has been estimated from the Monte Carlo simulation and is included in the quoted values.

The associated production of K^+K^- pairs results in a value of $R_{K^+K^-}$ of about 2. The values of $R_{K^+K^\circ}$ and $R_{K^-K^\circ}$ seem to indicate that the neutral kaons of undetermined strangeness are more frequently associated with negative than with positive kaons. The R_{ij} values corresponding to particles of the same nature (other than neutral kaons) are of the order of 0.4 as expected for uncorrelated pairs of low multiplicity particles. Here again, the agreement between the data and the Lund model predictions is good, within the statistical uncertainties.

We now turn to the associated production of $\Lambda\bar{\Lambda}$ pairs in order to investigate the production rate of strange diquarks in the fragmentation process. The 6 $\Lambda\bar{\Lambda}$ pairs (3 in H_2, 3 in D_2) and the 7 $\Lambda\Lambda$ pairs (4 in H_2, 3 in D_2) correspond to the following average multiplicities, corrected for acceptance and unseen decay modes:

$$\langle n(\Lambda\bar{\Lambda})\rangle = (4.7 \pm 2.1)\cdot 10^{-3}$$

$$\langle n(\Lambda\Lambda)\rangle = (2.6 \pm 1.2)\cdot 10^{-3} \ .$$

It should be noted that the average W for $\Lambda\bar{\Lambda}$ events is somewhat higher than for normal events (16.4 ± 2 GeV vs. 13.2 GeV).

In the two dimensional plot $\langle n(\Lambda\bar{\Lambda})\rangle$ versus $\langle n(\bar{\Lambda})\rangle$ (fig. 8), the Lund model predictions, for fixed γ_s/γ_u, fall on a straight line at a position depending on the value of the relative strange diquark suppression factor

$$R_{us} = (\gamma_{us}/\gamma_{ud})/(\gamma_s/\gamma_u).$$

For $\gamma_s/\gamma_u = 0.3$ which is the value in best agreement with the multiplicities presented in the previous section, our results favour a strong suppression factor (fig. 8).

This result shows that the particles in the observed $\Lambda\bar{\Lambda}$ pairs may well be produced independently with the Λ coming, for instance, from the target fragmentation and the $\bar{\Lambda}$ from some baryon-antibaryon pair production. This interpretation is already suggested by the fact that about equal numbers of $\Lambda\Lambda$ and $\Lambda\bar{\Lambda}$ pairs are produced. In e^+e^- annihilations where the measurement of $\Lambda\bar{\Lambda}$ pairs is directly related to R_{us}, a strong suppression has also been found at W=29 GeV [12].

6. Search for Short Range Correlations

The observation of short range correlations between charged kaons is difficult in this experiment due to the lack of acceptance around y=0 (see fig. 2). For this reason and with the kinematic range limited to 6 units of rapidity, the kaons from any observed pair are either close in rapidity or fall in opposite hemispheres. To avoid this experimental bias, we compare the mean kaon rapidity for event subsamples defined by the presence of another kaon of the same or opposite sign ("trigger" kaon).

The mean rapidity (fig. 9) is found to increase systematically with the rapidity of the trigger particle when the latter is of opposite sign. When the trigger particle is of the same sign, little dependence is seen. The data in fig. 9 is not corrected for acceptance and the observed structures are obviously influenced by kinematic constraints. For this reason, the observed features should be compared with those obtained for Monte Carlo events processed in the same way as the data. The latter are also shown in fig. 9 in the form of lines and exhibit similar features. This indicates that K^+ and K^- are produced closer in rapidity than same sign kaons, as expected from chain fragmentation.

7. Conclusions

The analysis of strange particle production in deep inelastic scattering of 280 GeV muons on hydrogen and deuterium leads to the following conclusions:

- The expected features of the basic quark-parton model, that the interaction takes place mostly on a u valence quark for $x_{Bj}>0.2$, are clearly observed in the data: positive kaons are more abundant than negative kaons over the full range of rapidity and Λ production occurs predominantly in the backward hemisphere. No significant differences are observed between the hydrogen and deuterium data.

- The parameterisation of the fragmentation process provided by the Lund string model with a strange to non-strange quark suppression of ≈ 0.3 is in good agreement with the observed K^+, K^- and $\bar{\Lambda}$ rates and spectra. For $6<W<20$ GeV, the best estimate of the strange quark suppression factor is:

$$\gamma_s/\gamma_u = 0.30 \pm 0.01 \text{ (stat.)} \pm 0.07 \text{ (syst.)}.$$

  The observed Λ spectrum is lower than the model prediction in the backward hemisphere.

- The distribution of the total average strangeness compensation along the rapidity axis shows a large asymmetry with an excess of negative strangeness in the backward hemisphere (Λ production from target remnants) and positive strangeness in the forward hemisphere (K^+ from the current u quark fragmentation). This asymmetry vanishes at low x_{Bj}.

- The measured $\Lambda\bar{\Lambda}$ pair production rate indicates a strong suppression of the strange versus non-strange diquark production and confirms the results obtained in e^+e^- annihilation.

- The rapidity distributions from K^+K^- pairs show that such pairs are produced closer in rapidity space than pairs of the same sign.

Acknowledgements

We would like to thank all the people in the various laboratories who have contributed to the construction, operation and analysis of this experiment. The support of the CERN staff in operating the SPS, muon beam and computer facilities is gratefully acknowledged.

References

[1] P. Renton and W.S.C. Williams, Ann. Rev. Nucl. Part. Sci. 31 (1981) 193;
J. Drees and H.E. Montgomery, Ann. Rev. Nucl. Part. Sci. 33 (1983) 383;
F. Dydak, Proceedings of the 1983 International Lepton/Photon Symposium, Cornell University, p.634.

[2] R.D. Field and R.P. Feynman, Nucl. Phys. B136 (1978) 1;
A. Ali et al., Phys. Lett. 93B (1980) 155.

[3] G. Ingelman et al., Nucl. Phys. B206 (1982) 239;
B. Andersson et al., Phys. Rep. 97 (1983) 31.

[4] S.L. Wu, Phys. Rep. 107 (1984) 59;
TASSO, M. Althoff et al., Z. Phys. C27 (1985) 27.

[5] EMC, J.J. Aubert et al., Phys. Lett. 103B (1981) 388;
EMC, J.J. Aubert et al., Z. Phys. C18 (1983) 189;
EMC, J.J. Aubert et al., Phys. Lett. 133B (1983) 370;
EMC, J.J. Aubert et al., Phys. Lett. 135B (1984) 225.

[6] EMC, M. Arneodo et al., Phys. Lett. 145B (1984) 156.

[7] EMC, M. Arneodo et al., Phys. Lett. 150B (1985) 458.

[8] EMC, O.C. Allkofer et al., Nucl. Instr. Meth. 179 (1981) 445;
EMC, J.P. Albanese et al., Nucl. Instr. Meth. 212 (1983) 111.

[9] a) A. Wroblewski, Acta Phys. Polonica B16 (1985) 379;
b) A. Breakstone et al., Phys. Lett. 135B (1984) 510;
c) T. Müller, Proceedings of the XIVth International Symposium on Multiparticle Dynamics, Lake Tahoe (June 1983), World Scientific Publishing Co., Singapore 1984, p.528.

[10] EMC, J.P. Albanese et al., Phys. Lett. 144B (1984) 302.

[11] EMC, M. Arneodo et al., Nucl. Phys. B258 (1985) 249.

[12] H. Aihara et al., Phys. Rev. Lett. 54 (1985) 274.

Table 1

Average Multiplicities of Strange Particles in Hydrogen versus W
The errors given are the statistical errors only.

W(GeV)	$\langle n_{K^+} \rangle$	$\langle n_{K^-} \rangle$	$\langle n_{K^\circ+\bar{K}^\circ} \rangle$	$\langle n_{\Lambda} \rangle$	$\langle n_{\bar{\Lambda}} \rangle$	$\langle n_{h^\pm} \rangle$ (Ref. 11)
4-6	0.15±.03	0.04±.01	0.17±.04	0.050±.012	0.010±.005	4.51±0.09
6-8	0.23±.03	0.14±.02	0.27±.04	0.056±.011	0.010±.003	5.10±0.05
8-10	0.30±.03	0.17±.02	0.32±.04	0.056±.011	0.019±.006	5.55±0.04
10-12	0.37±.03	0.25±.03	0.41±.04	0.087±.014	0.033±.007	6.06±0.04
12-14	0.34±.03	0.28±.02	0.42±.04	0.068±.012	0.029±.008	6.55±0.06
14-16	0.51±.03	0.33±.02	0.46±.04	0.079±.013	0.036±.009	6.95±0.08
16-18	0.39±.03	0.31±.02	0.54±.05	0.122±.017	0.027±.007	7.18±0.05
18-20	0.44±.03	0.48±.03	0.58±.05	0.076±.011	0.045±.010	7.38±0.10

Table 2

Ratios of Multiplicities versus W

The errors given are the statistical errors only.

$$R_1 = \frac{\langle n_{K^+} \rangle + \langle n_{K^-} \rangle + \langle n_{K^\circ + \bar{K}^\circ} \rangle}{\langle n_{h^\pm} \rangle}$$

W(GeV)	R_1 Data	R_1 Lund
4-6	0.08±.01	0.14
6-8	0.14±.01	0.16
8-10	0.14±.01	0.16
10.12	0.17±.01	0.17
12-14	0.16±.01	0.17
14-16	0.19±.01	0.17
16-18	0.17±.01	0.18
18-20	0.20±.01	0.18

Table 3

Number of strange particle pairs and global correlation factors R_{ij}

	K^+K^+	K^+K^-	K^+K°	$K^+\Lambda$	$K^+\bar{\Lambda}$
#	39	147	76	33	17
R_{ij}	0.35±0.06	1.93±0.18	1.31±0.16	1.42±0.27	1.00±0.31
R_{ij} Lund	0.39	2.69	1.51	2.23	0.63

	K^-K^-	K^-K°	$K^-\Lambda$	$K^+\bar{\Lambda}$
#	22	89	32	12
R_{ij}	0.35±0.08	1.54±0.20	1.13±0.23	1.32±0.44
R_{ij} Lund	0.38	1.65	0.78	1.69

	$K^\circ K^\circ$	$K^\circ\Lambda$	$K^\circ\bar{\Lambda}$
#	65	39	24
R_{ij}	1.06±0.15	1.87±0.33	2.15±0.56
R_{ij} Lund	0.82	1.61	1.12

	$\Lambda\Lambda$	$\Lambda\bar{\Lambda}$
#	7	6
R_{ij}	0.44±0.21	2.9±1.3
R_{ij} Lund	0.12	4.7

Figure Captions

Fig. 1 Ranges of momentum for which charged kaon identification is possible by the various identification detectors and corresponding acceptances.

Fig. 2 Acceptance for charged kaons (a-b), K° (c), Λ (d) and $\bar{\Lambda}$ (e) versus cms rapidity y . The acceptances for neutrals shown here do not include factors for branching ratios or K°_L decays.

Fig. 3 Normalised x_F distributions for K^+ (a), K^- (b), $K^\circ+\bar{K}^\circ$ (c), Λ's (d) and $\bar{\Lambda}$'s (e). Black dots are for the hydrogen target, open circles are for the deuterium target. As for all subsequent plots, quoted errors do not include systematic uncertainties (see text).

Fig. 4 Normalised cms rapidity distributions for K^+ (a), K^- (b) $K^\circ+\bar{K}^\circ$, (c), Λ (d) and $\bar{\Lambda}$ (e) for the merged hydrogen and deuterium data sets. The curves show the predictions of the Lund fragmentation model for values of the parameters quoted in section 3.2.

Fig. 5 (a) Normalised cms rapidity distribution of average strangeness separately for mesons (K^+-K^- in black dots) and for baryons ($\bar{\Lambda}$-Λ in open circles).
(b) Normalised cms rapidity distribution of the total observable strangeness <S>. The curves show the Lund model predictions.
(c) The average strangeness measured in the forward (black dots) and in the backward hemisphere (open circles) versus x_{Bj}. These average multiplicities are obtained by integrating on restricted rapidity ranges, forward: y>0.6 and backward: y<-0.6. The curves correspond to the Lund model predictions (forward: full line, backward: dotted line).

Fig. 6 Ratio of the average total kaon multiplicity to the total charged particle multiplicity as a function of W. The curves correspond to the Lund model predictions for γ_s/γ_u values of 0.25, 0.3 and 0.35.

Fig. 7. Values of γ_s/γ_u determined in various experiments [9].

Fig. 8. The average multiplicity of $\Lambda\bar{\Lambda}$ pairs versus the average $\bar{\Lambda}$ multiplicity and the Lund model predictions for different values of the strange diquark suppression factor R_{us} = 0., 0.2, 0.5 and 1. and for the value γ_s/γ_u = 0.3.

Fig. 9. The mean cms rapidity of charged kaons for events with an other kaon ("trigger") versus the cms rapidity of this trigger kaon. The lines show the values obtained from events generated according to the Lund model and modified by experimental acceptances and efficiencies.

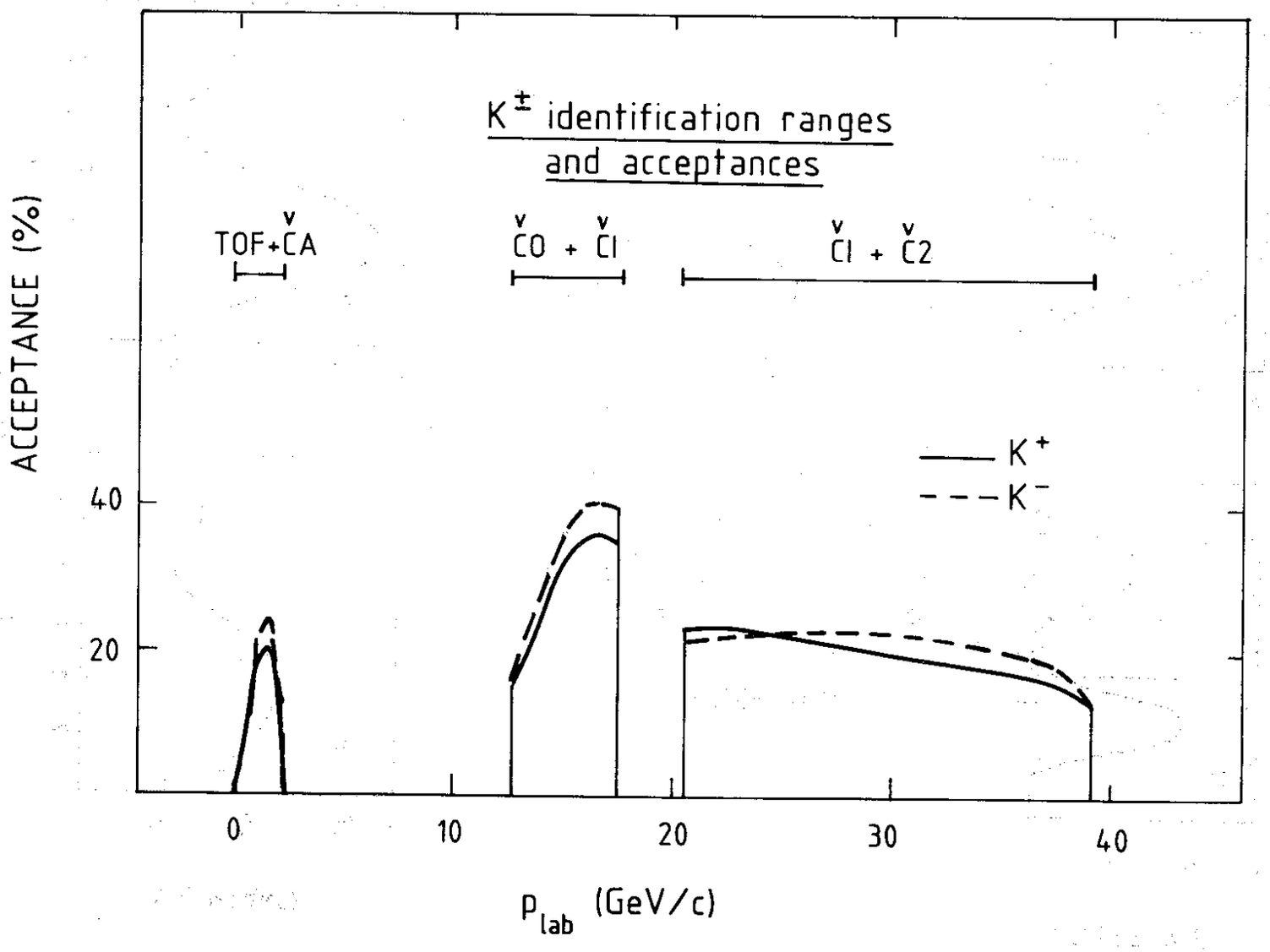
K± identification ranges
and acceptances
TOF+C̄A
C̄O + C̄I
C̄I + C̄2
K+
K−
ACCEPTANCE (%)
40
20
0
10
20
30
40
p lab (GeV/c)

FIG. 1

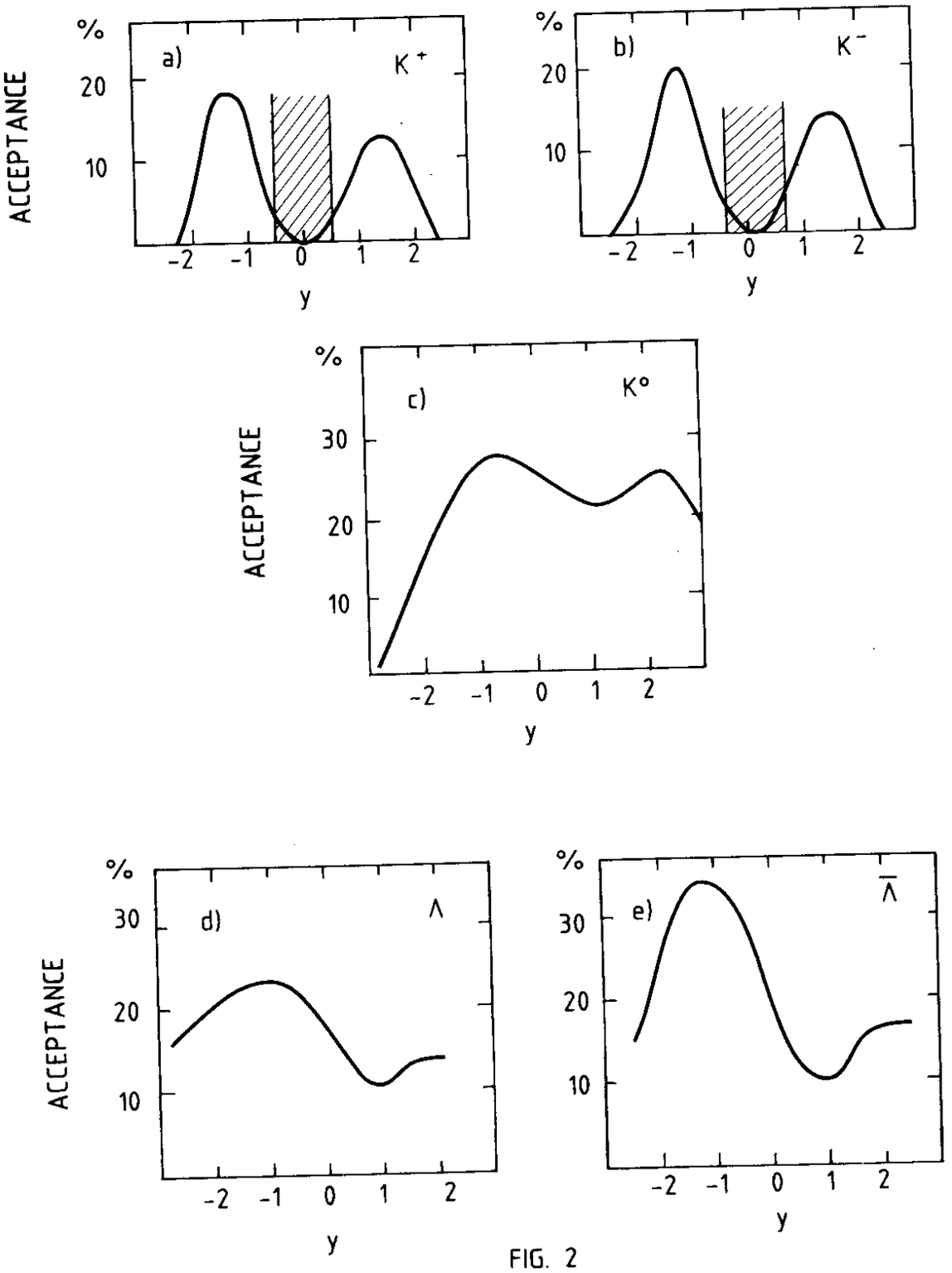
ACCEPTANCE
%
a)
K+
20
10
-2
-1
0
1
2
y
%
b)
K-
20
10
-2
-1
0
1
2
y
%
c)
K°
ACCEPTANCE
30
20
10
-2
-1
0
1
2
y
ACCEPTANCE
%
d)
Λ
30
20
10
-2
-1
0
1
2
y
%
e)
Λ̄
30
20
10
-2
-1
0
1
2
y

FIG. 2

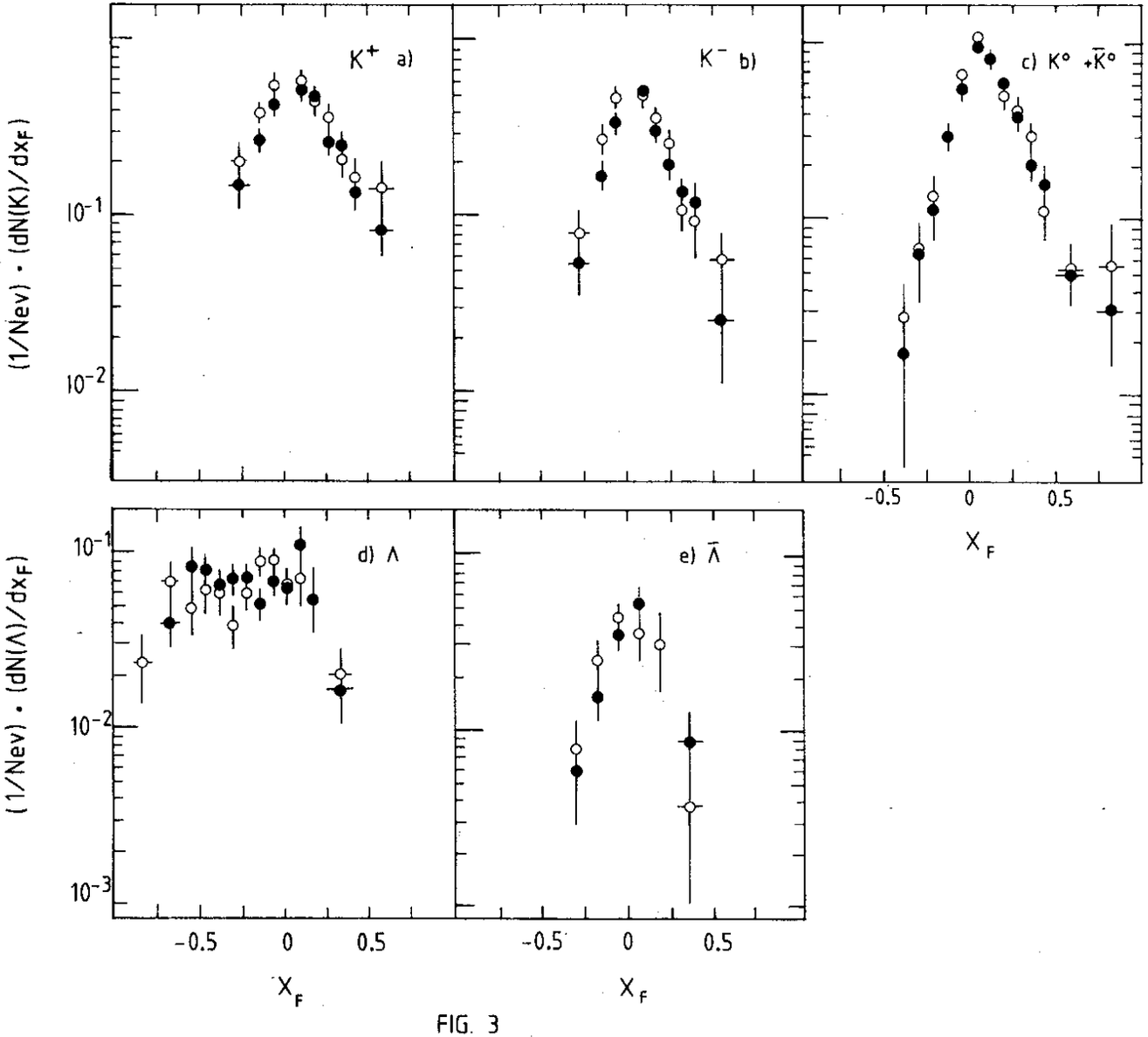

FIG. 3

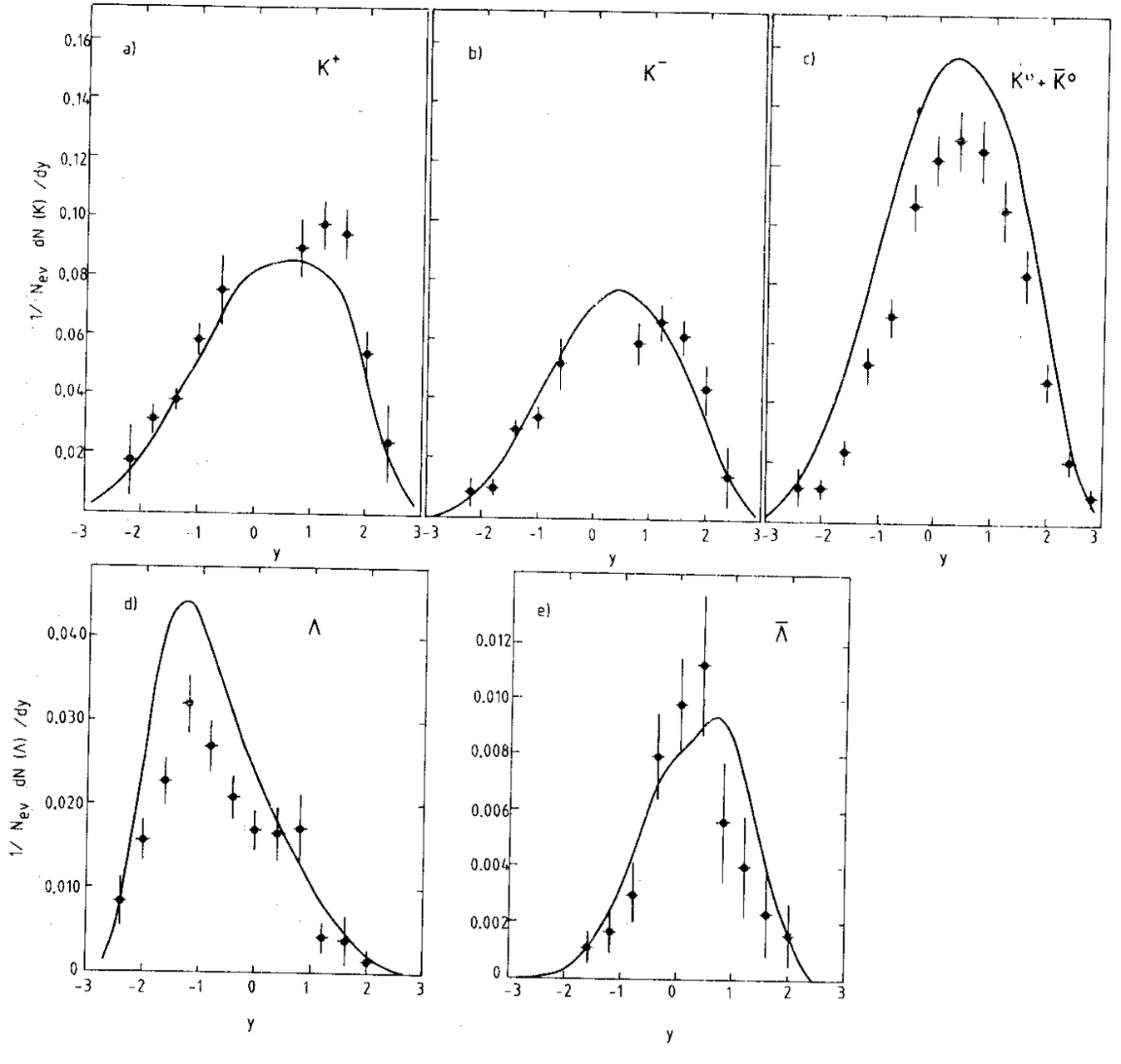
a)
K^+
b)
K^-
c)
$K^0 + \bar{K}^0$
d)
Λ
e)
$\bar{\Lambda}$
1/ N_{ev} dN (K) /dy
1/ N_{ev} dN (Λ) /dy
y

Fig.4

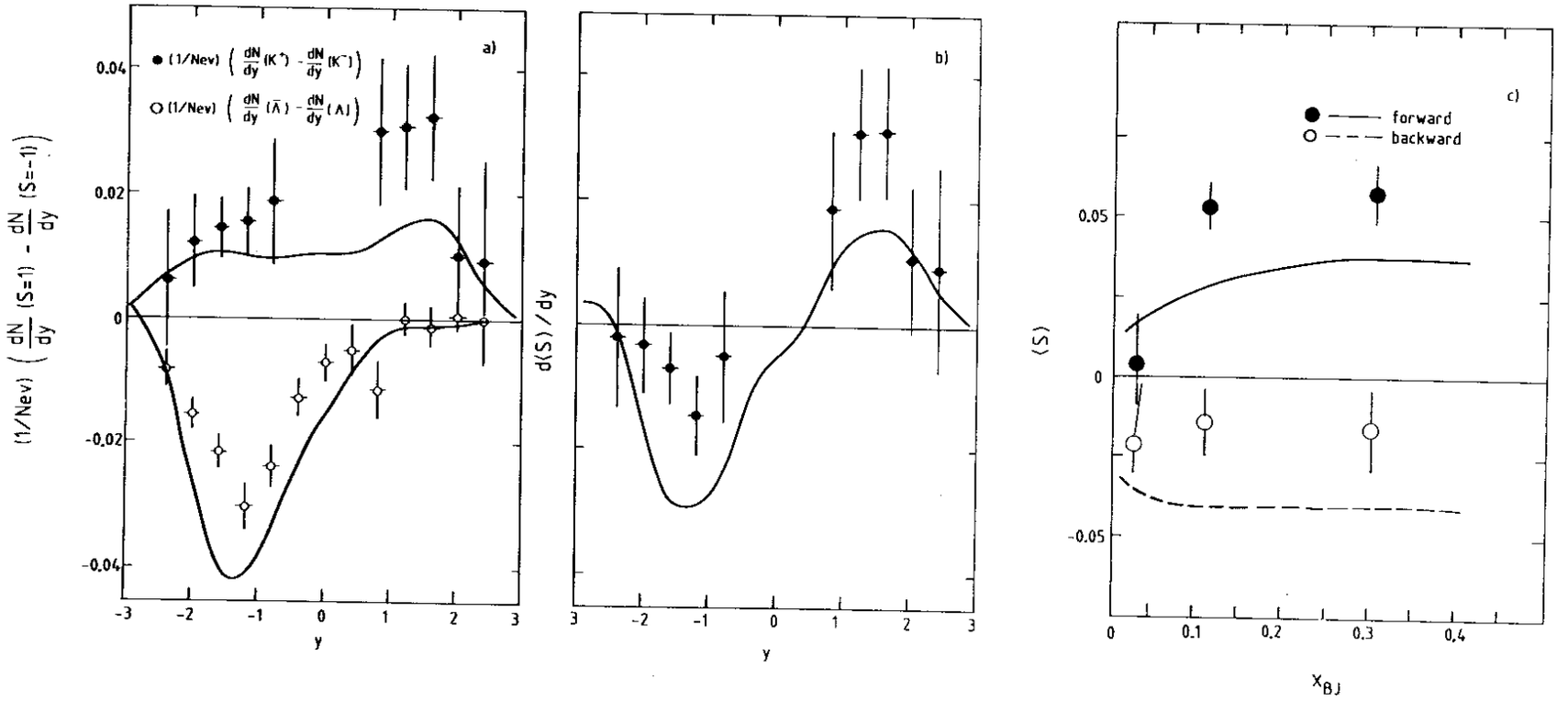
a)
b)
c)
(1/Nev) (dN/dy (S=1) - dN/dy (S=-1))
d(S) / dy
⟨S⟩
y
y
x_{BJ}
forward
backward
0.04
0.02
0
-0.02
-0.04
0.05
-0.05
0.1
0.2
0.3
0.4

FIG. 5

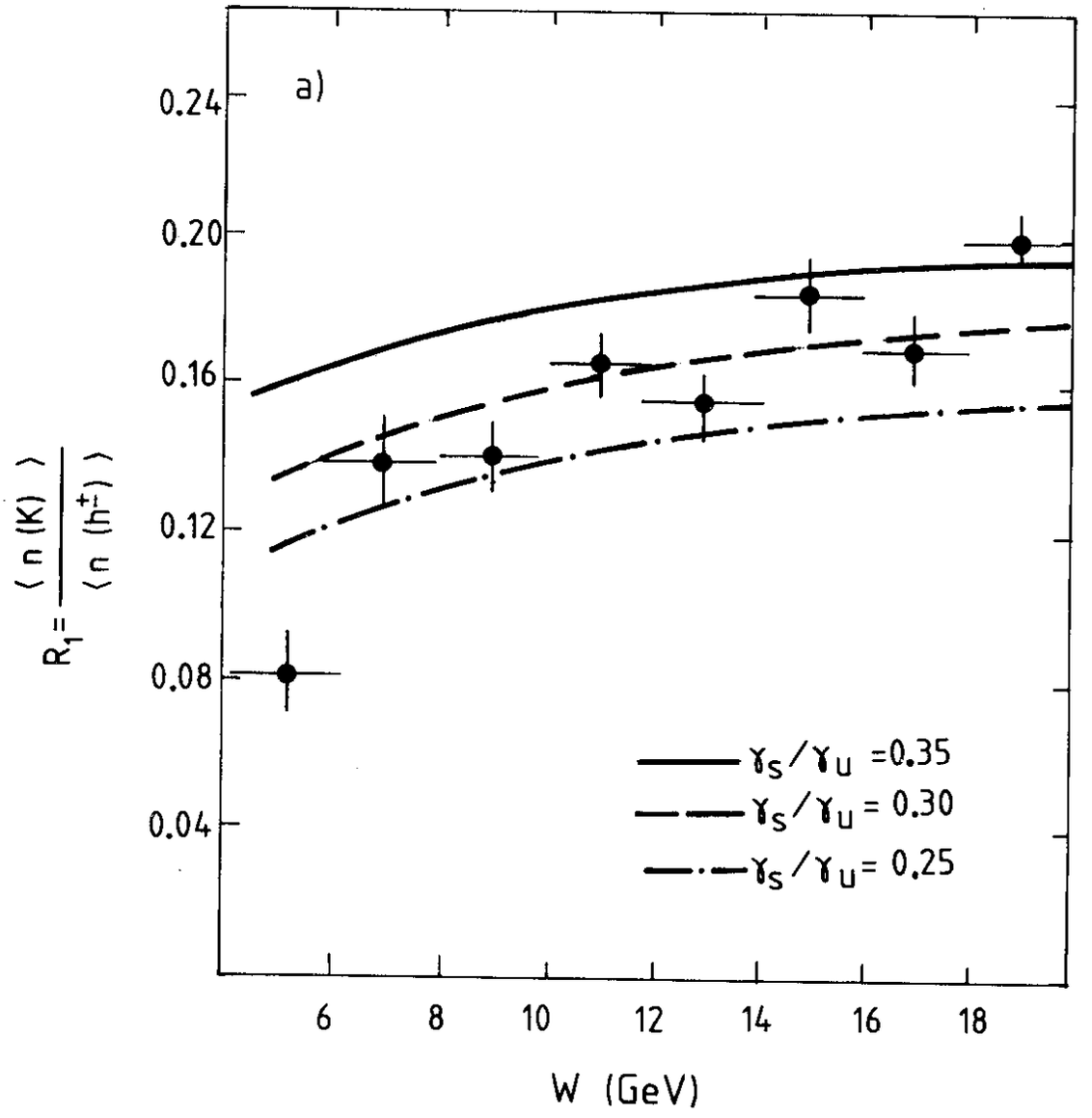
a)
0.24
0.20
0.16
0.12
0.08
0.04
$R_1 = \frac{\langle n(K) \rangle}{\langle n(h^{\pm}) \rangle}$
γ_s/γ_u =0.35
γ_s/γ_u = 0.30
γ_s/γ_u = 0.25
6
8
10
12
14
16
18
W (GeV)

FIG. 6

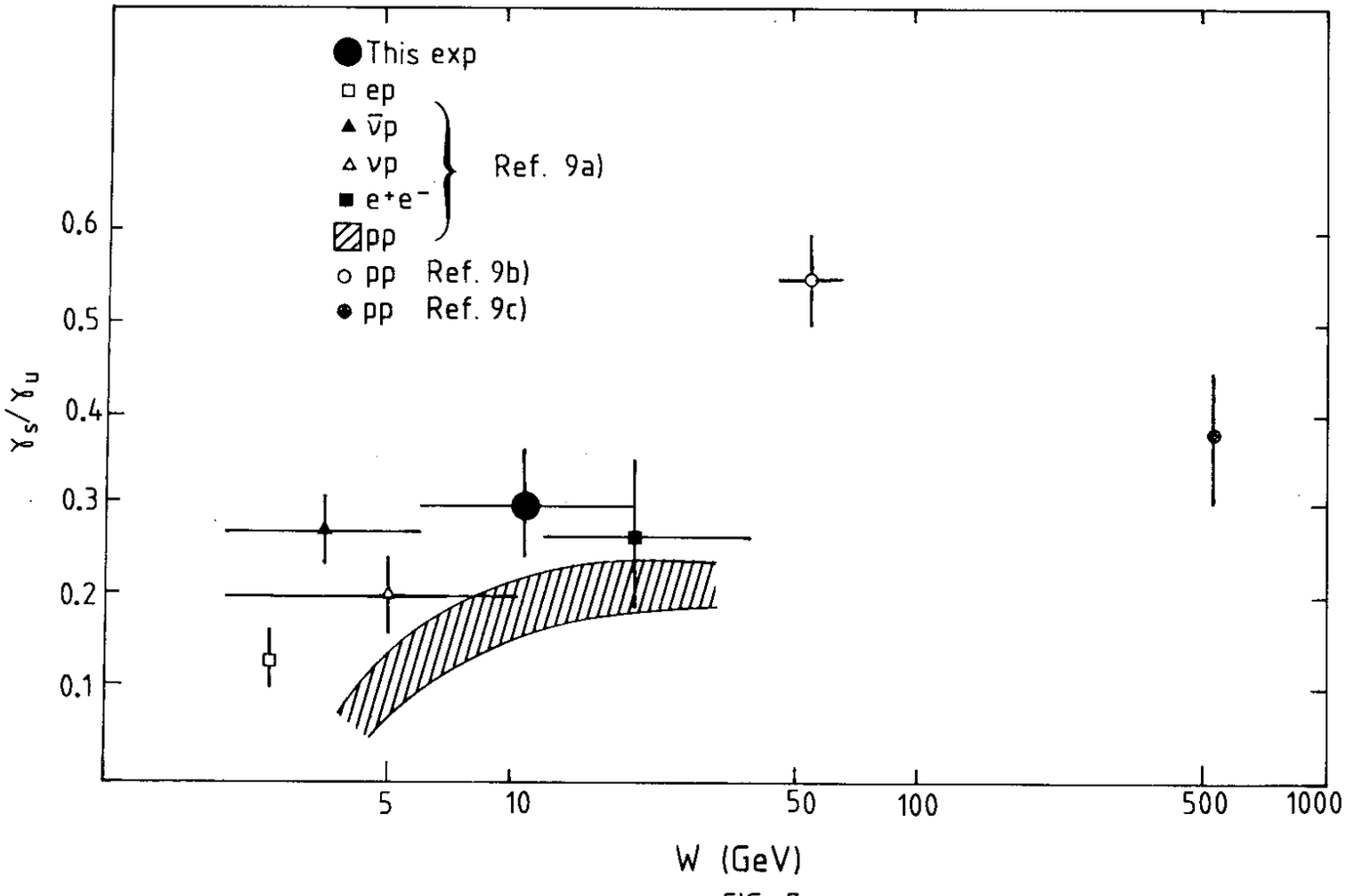
This exp
ep
$\bar{\nu}p$
νp
e^+e^-
Ref. 9a)
pp
pp Ref. 9b)
pp Ref. 9c)
γ_s/γ_u
0.6
0.5
0.4
0.3
0.2
0.1
5
10
50
100
500
1000
W (GeV)

FIG. 7

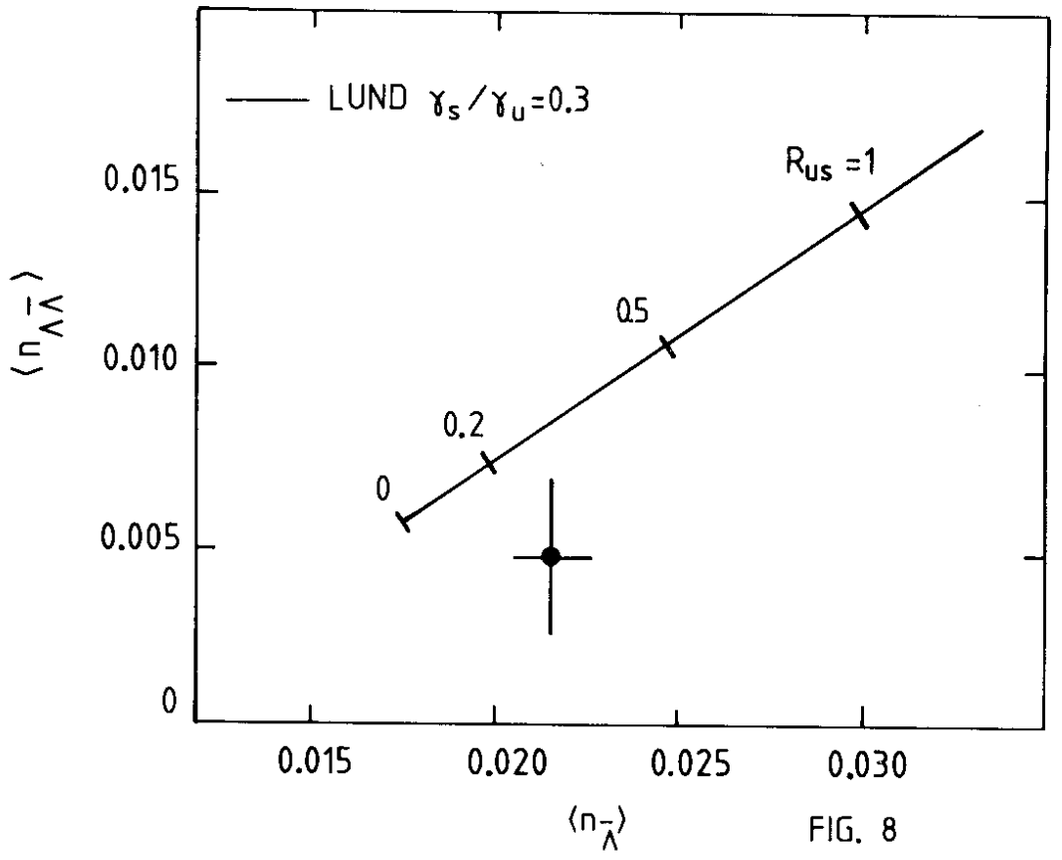
LUND γ_s/γ_u=0.3
R_{us} =1
0.5
0.2
0
0.015
0.010
0.005
0
0.015
0.020
0.025
0.030
$\langle n_{\bar{\Lambda}} \rangle$
$\langle n_{\bar{\Lambda}u} \rangle$

FIG. 8

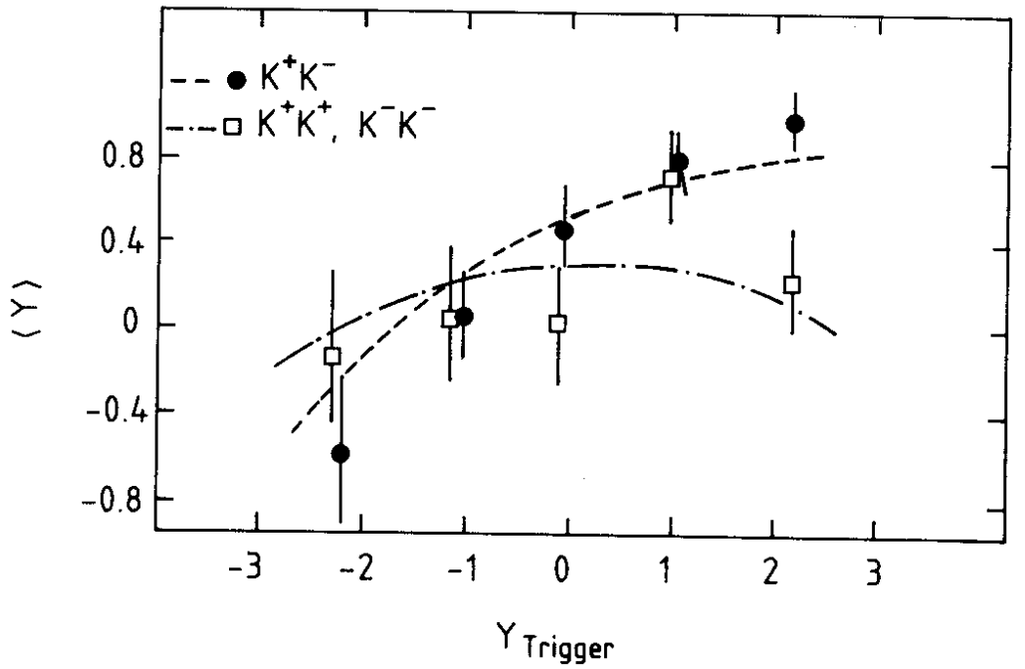
K^+K^-
K^+K^+, K^-K^-
0.8
0.4
0
-0.4
-0.8
-3
-2
-1
0
1
2
3
$\langle Y \rangle$
$Y_{Trigger}$

FIG. 9